Rapid Assessment of Size, Shape, and Chemical Complementarity of Ligands for Computational Protein Design

Rokas Petrenas[1*], Katarzyna Ożga[1], Joel J. Chubb[1], Andrey V. Romanyuk[1], Jennifer J. McManus[1], Graham J. Leggett[2], Nigel S. Scrutton[3], Thomas A. A. Oliver[1], Derek N. Woolfson[1]

[1]University of Bristol, [2]University of Sheffield, [3]University of Manchester
*rokas.petrenas@bristol.ac.uk https://doi.org/10.17952/38EPS.2026.P081

Overview

Driven by deep-learning approaches, computational protein design is advancing rapidly, and it is now possible to generate many *de novo* protein structures quickly and robustly.[1] This sets new frontiers for the field, including designing proteins that bind small molecules tightly and specifically, and understanding the non-covalent interactions that underpin such designs to make binding predictable and tunable. Here we address these challenges with a rapid physics-based computational method to generate isosteric and chemically complementary binding pockets for small-molecules in de novo designed coiled-coil peptides and proteins. We test this experimentally by constructing and characterising binding proteins for several synthetic and natural chromophores. For each ligand tested, the pipeline delivers stable proteins with pre-organised binding sites confirmed by X-ray crystallography, and micromolar binding affinities.

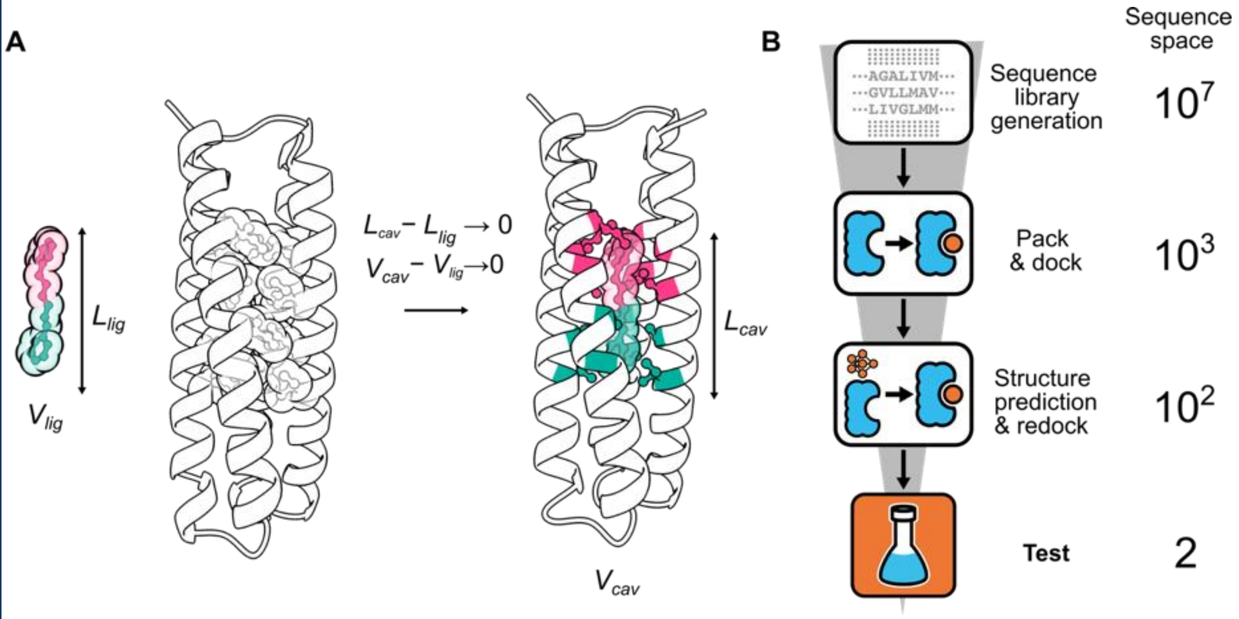


Figure 1. Design pipeline. (A) A binding site (L_{cav}) is identified based on the ligand length (L_{lig}). To match the ligand's shape, the protein scaffold is segmented (magenta and green). A volume constraint is used to minimise the difference between the binding cavity (V_{cav}) and the ligand (V_{lig}) in each segment; effectively, replacing atoms of the side chains with those of the ligand. (B) Sequences passing the volume constraint are packed onto the scaffold for evaluation using ligand docking, followed by modelling with AlphaFold2.

Delivering tight binding with sub-Å accuracy

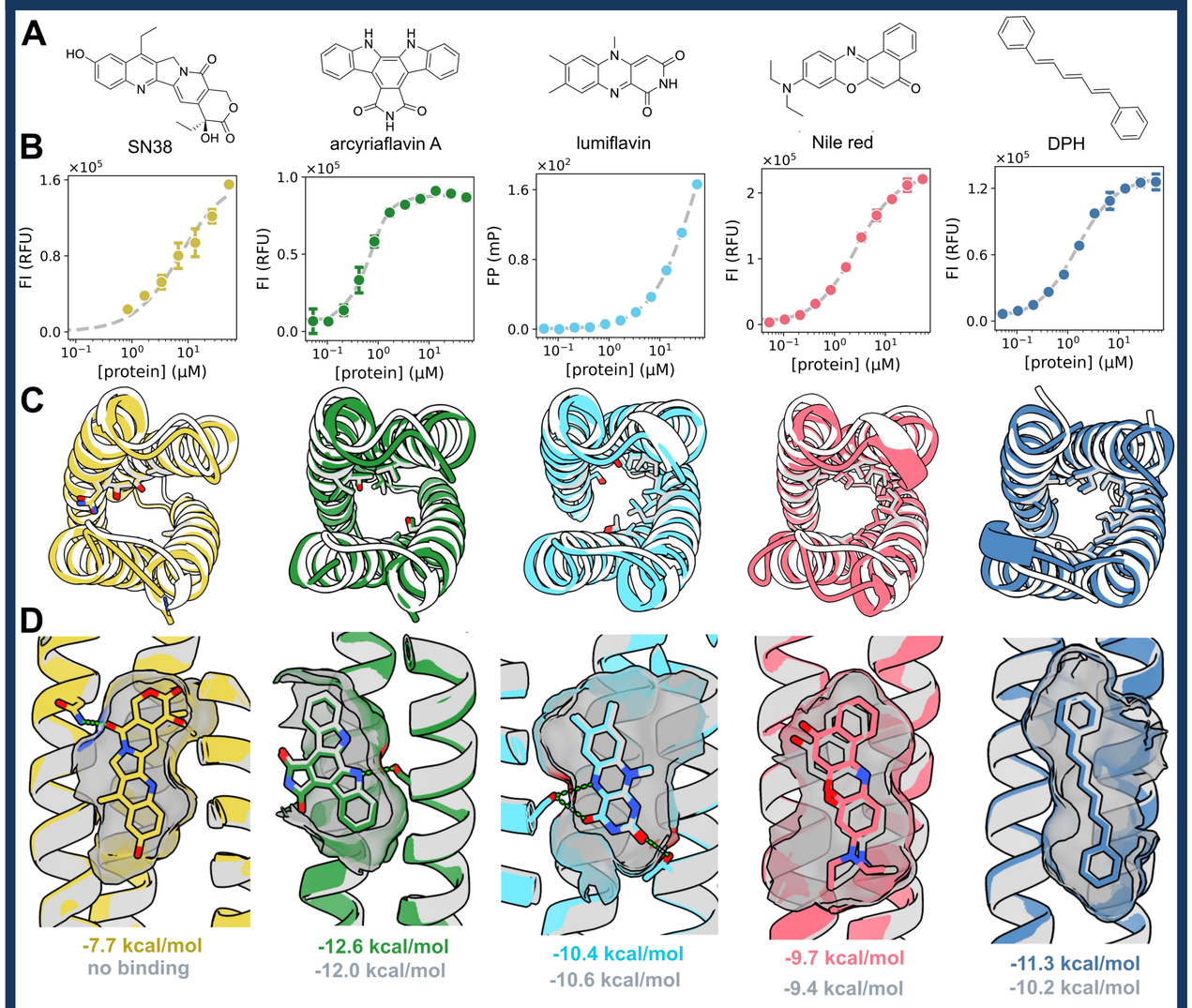


Figure 2. *De novo* designed binders for a wide range of ligands. (A) Ligands tested for binding. (B) Saturation-binding data measured by fluorescence intensity (FI) or fluorescence polarisation (FP) . Fitted dissociation constants, top to bottom: $K_{D(DPH)}$ = 1.25 ± 0.07 μM; $K_{D(Nile\ red)}$ = 2.4 ± 0.06 μM; $K_{D(lumiflavin)}$ = 51.64 ± 1.23 μM; $K_{D(arcyriaflavin\ A)}$ = 0.11 ± 0.02 μM; $K_{D(SN38)}$ = 6.92 ± 1.55 μM. (C) Binding-site heavy atom alignments between AF2 models (grey) and the ligand-free X-ray crystal structures. RMSD < 0.4 Å for all designs. (D) Docked poses and AutoDock Vina scores for the target ligands within the crystal structures, overlaid with the docked poses within the AF2 models (grey). Binding-site residues are highlighted and shown as sticks, with oxygen atoms in red and nitrogen atoms in blue. Hydrogen bonds are shown as dashed green lines.

Designs for *in vitro* and cellular applications

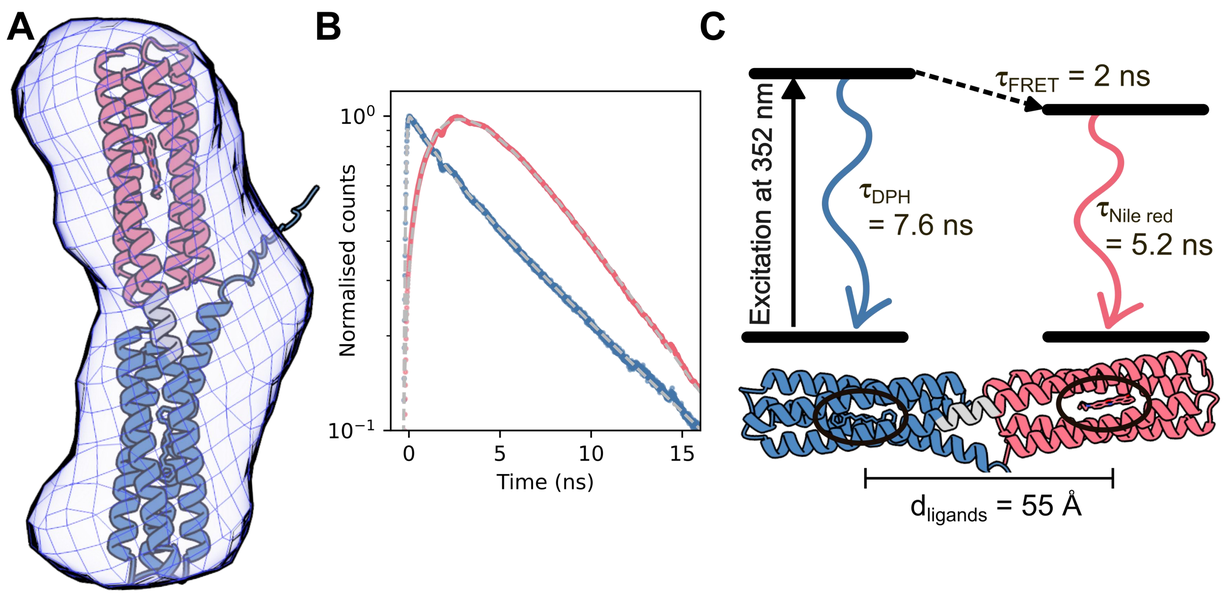


Figure 3. Dual binder promotes FRET between DPH and Nile red on a nanosecond scale. (A) AF2 model of the double-binder that combines DPH and Nile red binders, superposed to the averaged *ab initio* model from small angle X-ray scattering data. (B) Fluorescence lifetime decay measurements for DPH (blue, < 450 nm) and Nile red (red, >600 nm) after selective excitation of DPH at 352 nm. The delayed rise in Nile red emission over the first few nanoseconds originates from Förster resonance energy transfer between DPH and Nile red. (C) Kinetic model for energy transfer between DPH and Nile red, derived from (B).

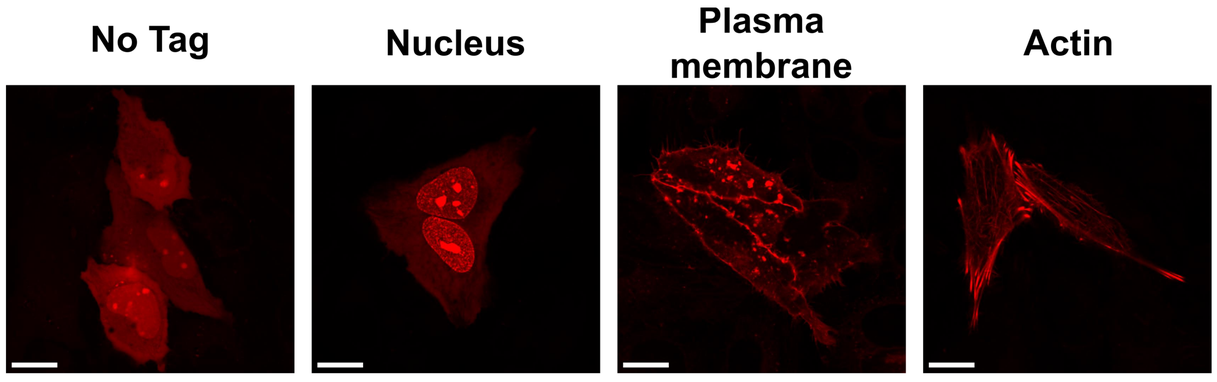


Figure 4. Nile red binder functions as a fluorescent reporter in mammalian cells. Fluorescence confocal microphotographs of live HeLa cells expressing the binder with N-terminal tags targeting the nucleus, plasma membrane and actin. Scalebar = 20 μm. Stained with 0.1 μM Nile red.

Controlling ligand specificity

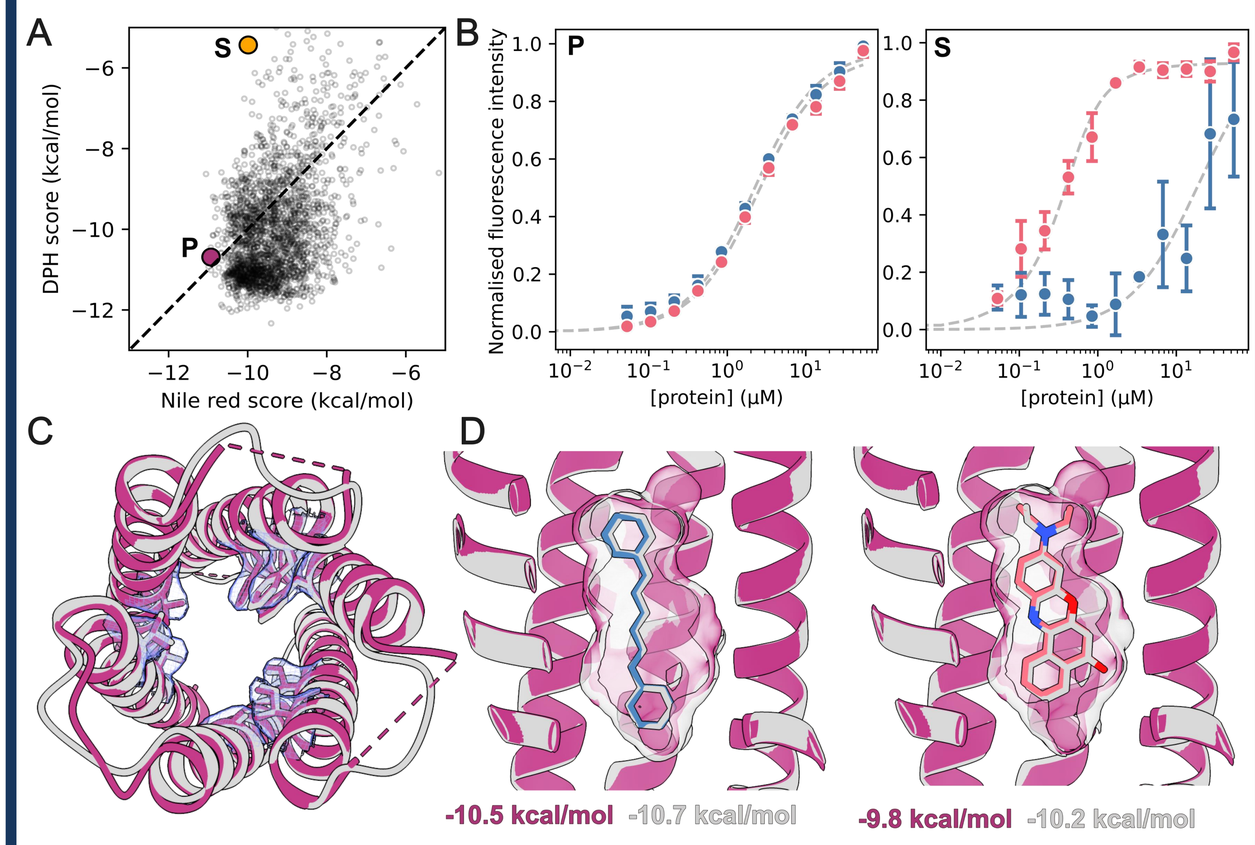


Figure 5. Designed promiscuous (P) and selective (S) binders for DPH and Nile red. (A) AutoDock Vina scores for DPH and Nile red docked into AF2 models. (B) Saturation binding curves and fits for Nile red (red) and DPH (blue) to the proteins. Promiscuous binder, $K_{D(DPH)}$ = 1.9 ± 0.17 μM; $K_{D(Nile\ red)}$ = 2.20 ± 0.17 μM. Specific binder, $K_{D(DPH)}$ > 20 μM; $K_{D(Nile\ red)}$ = 0.11 ± 0.04 μM. (C) Structural alignment between the AF2 model (grey) and the ligand-free X-ray crystal structure of the promiscuous binder. RMSD < 0.3 Å. (D) Docked poses of DPH and Nile red in the crystal structure of the promiscuous binder, overlaid with the docked poses within the AF2 models (grey).

SWBio DTP
UKRI Biotechnology and Biological Sciences Research Council
rosa biotech

References: [1] [a] E. A. Naudin, K. I. Albanese, A. J. Smith, B. Mylemans, E. G. Baker, O. D. Weiner, D. M. Andrews, N. Tigue, N. J. Savery, D. N. Woolfson, *Chem. Sci.*, **2022**, 13, 11330–11340. [b] K. I. Albanese, R. Petrenas, F. Pirro, E. A. Naudin, U. Borucu, W. M. Dawson, D. A. Scott, G. J. Leggett, O. D. Weiner, T. A. A. Oliver, D. N. Woolfson, *Nat. Chem. Biol.*, **2024**, 20, 991–999. [c] R. Petrenas, K. Ożga, J. J. Chubb, A. V. Romanyuk, J. J. McManus, G. J. Leggett, N. S. Scrutton, T. A. A. Oliver, D. N. Woolfson, *bioRxiv*, **2025**, 2025.06.30.662286.